REPORT DOCUMENTATION PAGE

Form Approved
OMB No. 0704-0188

1. AGENCY USE ONLY (Leave blank)	2. REPORT DATE	3. REPORT TYPE AND DATES COVERED
	June 1993	Technical

4. TITLE AND SUBTITLE

An HP-Adaptive Method in Space and Time for Parabolic Systems

5. FUNDING NUMBERS

DAAL03-91-G-0215

6. AUTHOR(S)

Joseph E. Flaherty
Peter K. Moore

7. PERFORMING ORGANIZATION NAME(S) AND ADDRESS(ES)

Rensselaer Polytechnic Institute
Troy, NY 12180-3590

8. PERFORMING ORGANIZATION REPORT NUMBER

9. SPONSORING / MONITORING AGENCY NAME(S) AND ADDRESS(ES)

U.S. Army Research Office
P.O. Box 12211
Research Triangle Park, NC 27709-2211

10. SPONSORING / MONITORING AGENCY REPORT NUMBER

ARO 29167.22-MA

11. SUPPLEMENTARY NOTES

The views, opinions and/or findings contained in this report are those of the author(s) and should not be construed as an official Department of the Army position, policy, or decision, unless so designated by other documentation.

12a. DISTRIBUTION / AVAILABILITY STATEMENT

Approved for public release; distribution unlimited.

12b. DISTRIBUTION CODE

13. ABSTRACT *(Maximum 200 words)*

ABSTRACT ON FIRST PAGE OF REPORT

14. SUBJECT TERMS

ON FIRST PAGE OF REPORT

15. NUMBER OF PAGES

35

16. PRICE CODE

17. SECURITY CLASSIFICATION OF REPORT	18. SECURITY CLASSIFICATION OF THIS PAGE	19. SECURITY CLASSIFICATION OF ABSTRACT	20. LIMITATION OF ABSTRACT
UNCLASSIFIED	UNCLASSIFIED	UNCLASSIFIED	UL

Rensselaer

Department of Computer Science
Technical Report

AN HP-ADAPTIVE METHOD IN SPACE AND TIME FOR PARABOLIC SYSTEMS

JOSEPH E. FLAHERTY AND PETER K. MOORE

Rensselaer Polytechnic Institute
Troy, New York 12180-3590

Report No. 93-15 **June 1993**

AN HP-ADAPTIVE METHOD IN SPACE AND TIME FOR PARABOLIC SYSTEMS*

JOSEPH E. FLAHERTY† AND PETER K. MOORE‡

Abstract. We describe an adaptive method-of-lines *hp*-refinement algorithm in space and time for one-dimensional vector systems of parabolic partial differential equations. Solutions are calculated using Galerkin's method with a piecewise-polynomial hierarchical basis in space and singly-implicit Runge-Kutta (SIRK) methods in time. A posteriori estimates of the local spatial and temporal discretization error are used with a priori error estimates to control spatial and temporal enrichment. Computational results are used to compare and verify the utility of several variants of the basic *hp*-refinement procedure.

Key words. adaptive refinement, finite-element methods, a posteriori error estimation.

MSC subject classifications. 65M20, 65M50, 65M60

1. Introduction. Basic adaptive strategies for the solution of parabolic partial differential equations (PDEs) include method-of-lines (MOL) approaches with spatial mesh refinement or coarsening (*h*-refinement) [1, 3, 5, 13, 18], mesh motion (*r*-

* This research was partially supported by the Board of Regents, LEQSF(1991-1993)-RD-A-32, by the U.S. Air Force Office of Scientific Research, Air Force Systems Command, USAF, under Grant Number AFOSR F49620-93-1-0218, and by the U.S. Army Research Office under Contract Number DAAL-03-91-G-0215.

† Department of Computer Science and Scientific Computation Research Center, Rensselaer Polytechnic Institute, Troy, New York 12180 and Benet Laboratories, Watervliet Arsenal, Watervliet, New York 12189

‡ Department of Mathematics, Tulane University, New Orleans, Louisiana 70118.

refinement) [1, 16], and order variation (p-refinement) [3, 14, 18]. Solution "enrichment indicators," which are frequently estimates of local spatial discretization errors [1-3, 5, 18, 21], are obtained from preliminary solutions and used to identify portions of the domain in need of additional resolution. Some combination of the three basic enrichment strategies is used to alter the approximation and recursively calculate improved solutions until specified accuracy criteria have been satisfied. The focus to date has been on h- and r-refinement [1-3, 5, 13, 16, 18] with little attention devoted to p- and hp-refinement [3, 19]. Since the latter schemes have been remarkably successful for elliptic problems it is natural to examine their utility when solving parabolic systems. With few exceptions [17], nothing has been done to coordinate spatial and temporal enrichment and we address a combined space-time adaptive hp-refinement strategy herein.

We consider vector systems of M parabolic equations of the form

$$\mathbf{u}_t + \mathbf{f}(x,t,\mathbf{u},\mathbf{u}_x) = \mathbf{D}(x,t,\mathbf{u},\mathbf{u}_x)_x, \quad x \in \Omega \equiv (c,d), \quad t > 0, \tag{1.1a}$$

$$\mathbf{u}(x,0) = \mathbf{u}_0(x), \quad x \in \Omega, \tag{1.1b}$$

$$u_i(x,t) = c_i(t) \quad x \in \partial\Omega_i^E, \tag{1.1c}$$

$$D_i(x,t,\mathbf{u},\mathbf{u}_x) = c_i(t), \quad x \in \partial\Omega_i^N, \quad i = 1, 2, \cdots, M, \quad t > 0. \tag{1.1d}$$

The boundary $\partial\Omega = \partial\Omega_i^E + \partial\Omega_i^N$ is divided component-wise, $i = 1, 2, \cdots, M$, into sets where essential (E) and natural (N) data is applied. Additional restrictions must be placed on the functions $\mathbf{f}$ and $\mathbf{D}$ to ensure that (1.1) is a well-posed parabolic problem with a locally-isolated solution.

We solve (1.1) using a finite element Galerkin MOL technique with a piecewise polynomial hierarchical spatial basis of degree $p \geq 1$ and a singly implicit Runge-

Kutta (SIRK) method in time (§2). SIRKs are well-suited to adaptive computation which requires frequent restarts of the temporal integration due to spatial enrichment, a consideration that would be even more important were local temporal refinement [18] used instead of a MOL. SIRKs additionally have high stage order that eliminates order reduction [11, 21] and error estimates of each stage that, with stability considerations, permit acceptance of solutions at intermediate stages whenever the final solution lacks the requisite accuracy [20].

A posteriori temporal (§3.1) and spatial (§3.2) error estimates are used to guide the adaptive *hp*-refinement algorithm as described in §4. A temporal order and step selection strategy (§4.1) is used to develop a *base* adaptive *hp*-refinement strategy and several variants (§4.2). Four examples are presented in §5. A comparison of the spatial *hp*-spatial refinement strategies of §4, an *h*-refinement strategy with various fixed orders (§4.2), and a p-refinement strategy with uniform spacing is made using a linear example. Burgers' equation is used to compare strategies for determining initial guesses for Newton's method and for comparing spatial *hp*-refinement strategies. A comparison of spatial *hp*-refinement strategies is also made using a Brusselator with some slight diffusion. The Brusselator [15] and a shear band model [12] demonstrate the effectiveness of our method on realistic nonlinear systems. A brief discussion of our results is presented in §6.

2. Discretization. The Galerkin form of (1.1) consists of determining $\mathbf{u}(x,t) \in H_E^1(\Omega) \times (t > 0)$ such that

$$(\mathbf{u}_t,\mathbf{v}) + (\mathbf{f},\mathbf{v}) + (\mathbf{D},\mathbf{v}_x) = \mathbf{D}^T\mathbf{v}\,|_{x \in \partial\Omega}, \quad \text{for all } \mathbf{v} \in H_0^1, \quad t > 0, \tag{2.1a}$$

$$(\mathbf{u},\mathbf{v}) = (\mathbf{u}_0,\mathbf{v}), \quad \text{for all } \mathbf{v} \in H_0^1, \quad t = 0, \tag{2.1b}$$

where

$$(\mathbf{u},\mathbf{v}) = \int_{\Omega} \mathbf{u}^T \mathbf{v} dx. \tag{2.1c}$$

As usual, the Sobolev space $H^1(\Omega)$ consists of functions having square integrable first derivatives and the subscripts E and 0 further restrict functions to satisfy (1.1c) and a trivial version of (1.1c), respectively.

Introduce a partition

$$\Delta_\Omega := \{c = x_0 < x_1 < \cdots < x_N = d\} \tag{2.2}$$

of Ω into N subintervals and approximate H^1 by a finite-dimensional subspace S^{Δ_Ω} where S^{Δ_Ω} consists of piecewise polynomials whose restriction to (x_{i-1},x_i) are polynomials of degree $p_i \geq 1$, $i = 1, 2, \cdots, N$. Consider a finite element approximation $\mathbf{U}(x,t) \in S_E^{\Delta_\Omega}$ of $\mathbf{u}(x,t) \in H_E^1$ having the form

$$\mathbf{U}(x,t) = \sum_{i=0}^{N} \overline{\mathbf{U}}_{i1}(t)\phi_{i1}(x) + \sum_{i=1}^{N} \sum_{k=2}^{p_i} \overline{\mathbf{U}}_{ik}(t)\phi_{ik}(x) \tag{2.3a}$$

where here, and throughout this paper, Galerkin coordinates are identified by an overbar. The functions

$$\phi_{ik}(x) = \begin{cases} (x - x_{i-1})/(x_i - x_{i-1}), & x_{i-1} \leq x < x_i \\ (x_{i+1} - x)/(x_{i+1} - x_i), & x_i \leq x < x_{i+1}, \quad i = 0, 1, \cdots, N, \quad k = 1, \\ 0, & \text{otherwise} \end{cases} \tag{2.3b}$$

and

$$\phi_{ik}(x) = \sqrt{\frac{2k-1}{2}} \frac{2}{x_i - x_{i-1}} \begin{cases} \int_{x_{i-1}}^{x} P_{i,k-1}(\nu)\, d\nu, & x_{i-1} \leq x < x_i \\ 0, & \text{otherwise} \end{cases},$$

$$i = 1, 2, \cdots, N, \quad k = 2, 3, \cdots, p_i, \tag{2.3c}$$

where $P_{i,k}(x)$ is the k^{th}-degree Legendre polynomial scaled to the subinterval

$[x_{i-1}, x_i]$, comprise a hierarchical basis for S^{Δ_Ω} [25].

In a similar manner, we approximate $\mathbf{v}$ by $\mathbf{V} \in S_0^{\Delta_\Omega}$; thus, replacing $\mathbf{u}$ and $\mathbf{v}$ in (2.1) by $\mathbf{U}$ and $\mathbf{V}$, we determine $\mathbf{U}(x,t)$ as the solution of the ordinary differential system

$$(\mathbf{U}_t,\mathbf{V}) + (\mathbf{f},\mathbf{V}) + (\mathbf{D},\mathbf{V}_x) = \mathbf{D}^T\mathbf{V}\,|_{x \in \partial\Omega}, \quad \text{for all } \mathbf{V} \in S_0^{\Delta_\Omega}, \quad t > 0, \tag{2.4a}$$

$$(\mathbf{U},\mathbf{V}) = (\mathbf{u}_0,\mathbf{V}), \quad \text{for all } \mathbf{V} \in S_0^{\Delta_\Omega}, \quad t = 0. \tag{2.4b}$$

Explicit utilization of (2.3) reveals that (2.4) has the form [20]

$$\mathbf{M}\bar{\mathbf{U}}' = \mathbf{F}(\bar{\mathbf{U}}), \quad t > 0, \quad \mathbf{M}\bar{\mathbf{U}}(0) = \mathbf{h}(\mathbf{u}_0), \tag{2.5a,b}$$

where $\mathbf{M}$, $\mathbf{F}$, and $\mathbf{h}$ are the mass matrix, load vector, and the initial load vector, respectively; $\bar{\mathbf{U}}(t)$ is a vector of Galerkin coordinates of length $n = M(N + 1 + \sum_{i=1}^{N}(p_i - 1))$ on $S_E^{\Delta_\Omega}$; and $(\,)'$ denotes total differentiation.

Implicit numerical methods are generally preferred for the temporal integration of systems like (2.5) that arise from parabolic problems. Stiffness arises in a MOL formulation due to the spatial discretization, so backward difference formulas (BDFs) are a common solution technique [1-3, 5, 17]. SIRKs, introduced by Butcher [9] and Norsett [22] and extended by Burrage [7], offer A-stability in combination with high-stage order and Jacobians of equal dimension to those of multistep methods; hence, they may provide an attractive alternative to BDF methods. We depart from Butcher's [9] SIRK procedure by approximating $\bar{\mathbf{U}}(t)$ rather than $\bar{\mathbf{U}}'(t)$ for the time step $[a, a + h]$ by an expression of the form

$$\bar{\mathbf{U}}(t) \approx \bar{\mathbf{W}}(t) = \sum_{l=0}^{s} \bar{\mathbf{W}}_l \psi_l(t), \quad \psi_l(t) = \sum_{m=0}^{s} \alpha_{lm} \left(\frac{t-a}{h}\right)^m, \tag{2.6a,b}$$

where the coefficients α_{lm}, $l, m = 0, 1, \cdots, s$, are given by Moore and Flaherty [20], $\overline{\mathbf{W}}_l = \overline{\mathbf{W}}(a+c_l h)$, $l = 1, 2, \cdots, s$, and $\overline{\mathbf{W}}_0 = \overline{\mathbf{W}}(a)$. Spatially-dependent functions $\mathbf{W}(x,t)$ and $\mathbf{W}_l(x)$, $l = 0, 1, \cdots, s$, may be defined by using $\overline{\mathbf{W}}(t)$ and $\overline{\mathbf{W}}_l$, $l = 0, 1, \cdots, s$, respectively, in conjunction with (2.3a-c).

The parameters c_l are selected as $\lambda\xi_l$, $l = 1, 2, \cdots, s$, where ξ_l is the l^{th} root of $L_s(t)$, the Laguerre polynomial of degree s. As described by Burrage [7], choosing λ as $1/\xi_{l^*}$, $1 \le l^* \le s$, can produce a method with favorable stability and discretization error properties. Using properties of Laguerre polynomials, Butcher [9] introduced the transformation

$$[\overline{\mathbf{W}}_1, \overline{\mathbf{W}}_2, \cdots, \overline{\mathbf{W}}_s]^T = \hat{\mathbf{T}}[\hat{\mathbf{W}}_1, \hat{\mathbf{W}}_2, \cdots, \hat{\mathbf{W}}_s]^T \tag{2.7a}$$

where $\hat{\mathbf{T}}$ is the tensor product of $\mathbf{T}$,

$$T_{ij} = L_{j-1}(\xi_i), \quad i, j = 1, 2, \cdots, s, \tag{2.7b}$$

with an $n \times n$ identity matrix that reduces the linearized version of (2.5a, 6) to the form [20]

$$\begin{bmatrix} \mathbf{M} - \lambda h \mathbf{F}_{\overline{\mathbf{U}}} & 0 & \cdots & 0 \\ \mathbf{M} & \mathbf{M} - \lambda h \mathbf{F}_{\overline{\mathbf{U}}} & \cdots & 0 \\ \cdot & \cdot & \cdots & \cdot \\ \cdot & \cdot & \cdots & \cdot \\ \mathbf{M} & \mathbf{M} & \cdots & \mathbf{M} - \lambda h \mathbf{F}_{\overline{\mathbf{U}}} \end{bmatrix} \begin{bmatrix} \Delta\hat{\mathbf{W}}_1 \\ \Delta\hat{\mathbf{W}}_2 \\ \cdot \\ \cdot \\ \Delta\hat{\mathbf{W}}_s \end{bmatrix} = - \begin{bmatrix} \hat{\mathbf{H}}_1 \\ \hat{\mathbf{H}}_2 \\ \cdot \\ \cdot \\ \hat{\mathbf{H}}_s \end{bmatrix} \tag{2.7c}$$

$$\begin{bmatrix} \hat{\mathbf{H}}_1 \\ \hat{\mathbf{H}}_2 \\ \cdot \\ \cdot \\ \hat{\mathbf{H}}_s \end{bmatrix} = - \begin{bmatrix} \mathbf{M}\overline{\mathbf{W}}_0 \\ \mathbf{M}\overline{\mathbf{W}}_0 \\ \cdot \\ \cdot \\ \mathbf{M}\overline{\mathbf{W}}_0 \end{bmatrix} + \begin{bmatrix} \mathbf{M} & 0 & \cdots & 0 \\ \mathbf{M} & \mathbf{M} & \cdots & 0 \\ \cdot & \cdot & \cdots & \cdot \\ \cdot & \cdot & \cdots & \cdot \\ \mathbf{M} & \mathbf{M} & \cdots & \mathbf{M} \end{bmatrix} \begin{bmatrix} \hat{\mathbf{W}}_1 \\ \hat{\mathbf{W}}_2 \\ \cdot \\ \cdot \\ \hat{\mathbf{W}}_s \end{bmatrix} - \lambda h \begin{bmatrix} \hat{\mathbf{F}}_1 \\ \hat{\mathbf{F}}_2 \\ \cdot \\ \cdot \\ \hat{\mathbf{F}}_s \end{bmatrix}. \tag{2.7d}$$

Thus, the Newton corrections $\Delta\hat{\mathbf{W}}_l$ to the transformed variables $\hat{\mathbf{W}}_l$,$l = 1, 2, \cdots, s$,

are determined by a simple block backward substitution involving s linear systems. Only one Jacobian is involved in all Runge-Kutta stages and inner products involving the lower diagonal entries in (2.7c,d) may be accumulated stage by stage. Additionally, the terms $\mathbf{M}\hat{\mathbf{W}}_l$, $l = 1, 2, \cdots, s$, in (2.7d), need not be evaluated after the initial Newton iteration since corrections of $\mathbf{M}\Delta\hat{\mathbf{W}}_l$, $l = 1, 2, \cdots, s$, are generated by (2.7c). Inverting (2.7b) to obtain $\overline{\mathbf{W}}_l$, $l = 1, 2, \cdots, s$, is straightforward [9]. By using the formulation (2.6-7) instead of Butcher's [9] original approach, we avoid solving an additional linear system by determining $\overline{\mathbf{W}}$ directly rather than obtaining it from $\mathbf{F}$.

With $\lambda = 1/\xi_{l^*}$, $1 \le l^* \le s$, we have $c_{l^*} = 1$; hence, $\overline{\mathbf{W}}(a+h) = \overline{\mathbf{W}}_{l^*}$ is regarded as the final-stage solution that is propagated to the next time step if accuracy conditions are satisfied. All other solutions $\overline{\mathbf{W}}_l$, $l = 1, 2, \cdots, l^* - 1, l^* + 1, \cdots, s$, furnish intermediate results. Moore and Flaherty's [20] stability analysis permits the acceptance of solutions at some intermediate stages for $l < l^*$. This is particularly useful when the discretization error of $\mathbf{W}_{l^*}$ is larger than prescribed but that of $\mathbf{W}_l$, $l < l^*$, is acceptable. Those stages that satisfy Moore and Flaherty's [20] stability conditions and, hence, may be propagated forward are called "acceptable stages." Acceptable stages with $l < l^*$ and, hence, $c_l < 1$ are referred to as "partial steps" while "full steps" are taken when $l = l^*$. For reference, we include the set of acceptable stages, Γ_s, $s = 1, 2, \cdots, 8$, in Table 2.1 [20]. For the adaptive algorithm of §4.2 it will also be useful to define the set of "adaptive stages" Ψ_s, $s = 1, 2, \cdots, 8$, as presented in Table 2.2.

s	1	2	3	4	5	6	7	8
Γ_s	{1}	{1,2}	{1,2}	{1,2}	{2,3}	{2,3}	{2,3,4}	{2,3,4}

Table 2.1. The set Γ_s of potentially acceptable stages for a s-stage SIRK, $s = 1, 2, \cdots, 8$.

s	1	2	3	4	5	6	7	8
Ψ_s	{1}	{1,2}	{1,2,3}	{1,2,3}	{2,3,4}	{2,3,4}	{2,3,4,5}	{2,3,4,5}

Table 2.2. The set Ψ_s of adaptive stages for a s-stage SIRK, $s = 1, 2, \cdots, 8$.

3. Error Estimation. The adaptive algorithms of §4 utilize estimates of the total error $\mathbf{e} = \mathbf{u} - \mathbf{W}$, the spatial error $\mathbf{e}^x = \mathbf{U} - \mathbf{W}$, and the temporal error $\mathbf{e}^t = \mathbf{u} - \mathbf{U}$. Procedures for estimating the total error [2, 21] are reviewed briefly for completeness. All estimates are calculated using the root-mean-square norm [6]

$$\|\mathbf{e}\|_{rms} = \sqrt{\frac{1}{M}\sum_{i=1}^{M} \frac{\|e^i\|_1^2}{(atol^i + rtol^i \|W^i\|_1)^2}} \tag{3.1}$$

where e^i is the i^{th} component of $\mathbf{e}$, and $atol^i$ and $rtol^i$, $i = 1, 2, \cdots, M$, are prescribed absolute and relative error tolerances, respectively. Temporal error estimation is the subject of §3.1 and spatial error estimation follows in §3.2.

3.1. Temporal Error Estimation. Temporal error estimates, which control step and order selection, can be obtained for all stages [8, 20] by embedding. The additional stage

$$\overline{\mathbf{W}}_{s+1} = \overline{\mathbf{W}}_0 - \sum_{k=1}^{s} [c_{s+1} L'_k(c_{s+1}/\lambda)/k + \lambda L_{k-1}(c_{s+1}/\lambda)] [\sum_{i=1}^{k} 1/\lambda \hat{\mathbf{W}}_i - \overline{\mathbf{W}}_0] + h\lambda \mathbf{F}(\overline{\mathbf{W}}_{s+1}), \tag{3.2}$$

furnishes higher-order temporal solutions that may be subtracted from existing solutions to obtain error estimates

$$\|\mathbf{e}^t(\cdot, a + c_l h)\|_{rms} \approx \|\mathbf{E}_l^t(\cdot)\|_{rms} \equiv \|L_{s+1}(c_l/\lambda)(\mathbf{W}_{s+1}(\cdot) - \mathbf{W}_0(\cdot))\|_{rms},$$

$$l = 1, 2, \cdots, s, \tag{3.3}$$

of all stages [20].

Estimates of the scaled derivatives $\|h^{s+k}\partial_t^{s+k}\mathbf{U}(\cdot,a+h)\|_{rms}$, $k=-1, 0, 1, 2$, are needed for the order selection strategy described in §4.1. Estimates of $h^{s-1}\partial_t^{s-1}\mathbf{U}(\cdot,a+h)$ and $h^s\partial_t^s\mathbf{U}(\cdot,a+h)$ are obtained by writing (2.6) in the form [20]

$$\overline{\mathbf{W}}(t)=\overline{\mathbf{W}}_0 L_s(\theta/\lambda)+\sum_{k=1}^{s}\hat{\mathbf{W}}_k[L_{k-1}(\theta/\lambda)-L_s(\theta/\lambda)],\quad \theta=\frac{t-a}{h} \tag{3.4a,b}$$

and differentiating $s-1$ and s times, respectively.

Results of Burrage et al. [8] imply that

$$\overline{\mathbf{E}}_l^t(t)=-h[\sum_{j=1}^{s}(b_j-\bar{b}_j)\mathbf{F}(\overline{\mathbf{W}}_j)-\bar{b}_{s+1}\mathbf{F}(\overline{\mathbf{W}}_{s+1})] \tag{3.5a}$$

where b_j, $j=1, 2, \cdots, s$, and $\bar{b}_j$, $j=1, 2, \cdots, s+1$, satisfy the consistency conditions

$$\sum_{j=1}^{s}b_j c_j^l=\frac{1}{l+1},\quad l=0, 1, \cdots, s-1,\quad \sum_{j=1}^{s+1}\bar{b}_j c_j^l=\frac{1}{l+1},\quad l=0, 1, \cdots, s. \tag{3.5b,c}$$

Using Taylor's series and (3.5b,c), it follows that

$$\begin{aligned} &h[\sum_{j=1}^{s}(b_j-\bar{b}_j)z(a+c_j h)-\bar{b}_{s+1}z(a+c_{s+1}h)] \\ &\quad=z^{(s)}(a)h^{s+1}\frac{1}{s!}[\sum_{j=1}^{s}b_j c_j^s-\frac{1}{s+1}] \end{aligned} \tag{3.6}$$

for any function $z(t)\in C^{s+1}[a,b]$. Extending (3.6) to vector systems with $\mathbf{z}=\overline{\mathbf{U}}'$ yields [8]

$$H^{s+1}\overline{\mathbf{U}}_l^{(s+1)}(a+h)=-\frac{\lambda^{s+1}\overline{\mathbf{E}}_l^t\cdot s!}{\sum_{j=1}^{s}b_j c_j^s-1/(s+1)}+O(H^{s+2}) \tag{3.7}$$

where $H=\lambda h$.

The final scaled derivative $H^{s+2}\overline{\mathbf{U}}_l^{(s+2)}(a+h)$ is estimated by taking two full

steps on the same spatial mesh with the same temporal order and time step and using (3.7) to show that [8]

$$H^{s+2}\bar{\mathbf{U}}_l^{(s+2)}(a+h) = \frac{\lambda^{s+2}\nabla\bar{\mathbf{E}}_{l\cdot}^{t}(a+h)s!}{\sum_{j=1}^{s} b_j c_j^s - 1/(s+1)} + O(H^{s+3}) \tag{3.8a}$$

where

$$\nabla\bar{\mathbf{E}}_{l\cdot}^{t}(a+h) = \bar{\mathbf{E}}_{l\cdot}^{t}(a+h) - \bar{\mathbf{E}}_{l\cdot}^{t}(a). \tag{3.8b}$$

3.2 Spatial Error Estimation. Estimates of the spatial and total discretization errors are obtained by computing two additional solutions

$$\mathbf{Y}^k(x,t) = \mathbf{W}(x,t) + \mathbf{E}^k(x,t), \quad \mathbf{E}^k(x,t) = \mathbf{E}^t(x,t) + \sum_{l=0}^{k} \mathbf{E}^{x,l}(x,t), \quad k = 0, 1, \tag{3.9a,b}$$

where $\mathbf{E}^k$ and $\mathbf{E}^{x,k}$ are, respectively, total and spatial error estimates of each solution $\mathbf{Y}^k$, $k = 0, 1$. The temporal error estimate $\mathbf{E}^t$, obtained as described in §3.1, is used for all acceptable SIRK stages, otherwise it is set to zero. The complexity of obtaining spatial error estimates may be reduced by using nodal superconvergence [2, 21]. Thus, errors on Δ_Ω are neglected and spatial errors are approximated by local p-refinement with

$$\mathbf{E}^{x,k}(x,t) = \sum_{i=1}^{N} \bar{\mathbf{E}}_i^{x,k}(t)\phi_{i,p_i+k+1}(x), \quad k = 0, 1, \tag{3.10a}$$

by replacing $\mathbf{u}$ in (2.1) by $\mathbf{Y}^k$, $k = 0, 1$, to obtain the local Galerkin problems

$$(\mathbf{Y}_t^k,\mathbf{V})_i + (\mathbf{f}(x,t,\mathbf{Y}^k,\mathbf{Y}_x^k),\mathbf{V})_i + (\mathbf{D}(x,t,\mathbf{Y}^k,\mathbf{Y}_x^k)_i = 0, \quad \text{for all } \mathbf{V} = \bar{S}_0^{p_i+k+1,(x_i-x_{i-1})},$$

$$t \in (a, a + c_s h), \quad i = 1, 2, \cdots, N, \tag{3.10b}$$

$$\mathbf{Y}^k(x,a) = \mathbf{W}(x,a), \quad k = 0,1. \tag{3.10c}$$

The problems (3.10b,c) are solved for $\mathbf{Y}^k$, $k = 0, 1$, using the same s-stage SIRK that was used to obtain the finite element solution $\mathbf{W}$. The local spaces $\bar{S}_0^{p_i+k+1,(x_i-x_{i-1})}$

consists of polynomials having maximal degree p_i+k+1, $k = 0, 1$, on (x_{i-1},x_i), $i = 1, 2, \cdots, N$. The local L^2 inner product $(\mathbf{u},\mathbf{v})_i$ is defined according to (2.1c) with Ω replaced by (x_{i-1},x_i).

The total error $\|e(\cdot,a + c_j h)\|_{rms}$, is approximated by $\|\mathbf{E}^0(\cdot,a + c_j h)\|_{rms}$, $j \in \Gamma_s$; however, the spatial order selection strategy (cf. §4.2) requires estimates of $\|\mathbf{E}^{x,k}(\cdot,a + c_j h)\|_{rms,i}$, $k = -2, -1, 0, 1$, $j \in \Psi_s$, $i = 1, 2, \cdots, N$. The estimates $\mathbf{E}^{x,0}$ and $\mathbf{E}^{x,1}$ are computed using (3.9,10). The errors $\mathbf{E}^{x,-1}$ and $\mathbf{E}^{x,-2}$ of solutions one and two degrees lower, respectively, than the current approximation on each element, are obtained naturally from the p_i^{th} and $p_i - 1^{st}$ terms of the hierarchical series (cf., e.g. (2.3)). This approach differs from the order extrapolation techniques for elliptic problems of Szabo [26] and Zienkiewicz et al. [29]. Unlike these procedures, availability of $\mathbf{Y}^1$ provides us with a rational basis to change orders from piecewise linear to piecewise quadratic solutions.

4. Adaptive Strategies. A top-level pseudo-C description of an adaptive MOL hp-refinement algorithm for solving (2.1) on $\Omega \times (0,T]$ is presented in Figure 4.1. Input to this procedure, called *MOLhp*, consists of T and absolute and relative error tolerance vectors **atol** and **rtol**, respectively. The core of *MOLhp* is the integration of (2.1) for a single time step of duration h. The temporal (§4.1) and spatial (§4.2) *hp*-refinement strategies are based on the order and step selection strategy used within the BDF code DASSL [6]. With both temporal and spatial enrichment, the order is chosen prior to selecting the step size.

4.1 Adaptive Strategies in Time. Current techniques for selecting the temporal order and step size (cf., e.g., Brenan et al. [6]) on a subinterval $(a,a+h]$ utilize estimates of the four scaled derivatives $\|h^{s+k}\partial_t^{s+k}\mathbf{U}(\cdot,a)\|_{rms}$, $k = -1, 0, 1, 2$, where s is the order of the previous step (cf. §3.1). The order is decreased or increased by one if the sequence of scaled derivatives at different orders is, respectively, decreasing or

MOLhp(**atol**, **rtol**, T)
{
$a = 0$;
Generate an initial mesh Δ_Ω and select an initial time step with $s = 1$;
while $(a + h \le T)$
{
Solve (2.5) on $(a, a+h] \times \Delta_\Omega$ using a s-stage SIRK to obtain the approximate solution $\mathbf{W}(x, a+h)$, the total error estimates $\mathbf{E}^0(x, a + c_l h)$, $l \in \Gamma_s$, and the spatial error estimates $\mathbf{E}^{x,k}(x, a + c_l h)$, $k = -2, -1, 0, 1$, $l \in \Psi_s$;
Use $\mathbf{E}^{x,k}(x, a + c_l h)$, $k = -2, -1, 0, 1$, $l \in \Psi_s$, to obtain the elemental spatial error indicators $I_i^{x,k}$, $i = 1, 2, \cdots, N$, $k = -2, -1, 0, 1$;
Determine $l_{\max} = \max_{l \in \Gamma_s} l$ such that $\|\mathbf{E}^0_{l_{\max}}\|_{rms} \le 1$;
If $(l_{\max} > 0)$
$a \mathrel{+}= c_{l_{\max}} h$;
Calculate a new time step h and SIRK order s;
if $(l_{\max} < l^*)$
Generate a new grid Δ_Ω based on the refinement indicators;
else
Generate a new grid Δ_Ω if significant refinement or coarsening is needed;
}
}

Figure 4.1. Pseudo-C description of the adaptive MOL algorithm with local hp-refinement for solving (2.1) on $\Omega \times (0,T]$.

increasing [6]. Once the order has been selected, the appropriate scaled derivative is used with the local discretization error formula to select the time step so that the temporal error estimate is less than 1/10 of the total error estimate [24]. A factor of 1/10 produced much more reliable results (cf. Example 5.4) than our previous factor of 1/3 [19]. If the temporal error estimate is too large, spatial error estimates may be unreliable due to inaccurate integration of (3.10). Thus, the time step is reduced without spatial adaptivity when the temporal error estimate is more than 20% of the total error estimate and the total error estimate is more than 0.8

Interpolation provides estimates of the solution at times other than $a + c_l h$, $l = 1, 2, \cdots, s$, which may, e.g., be used to compute initial guesses for Newton's iteration. The interpolation strategy used in the SIRK code STRIDE [8] satisfies (3.4) [20] and is denoted as $\overline{\mathbf{W}}_{BBC}(t)$. High-order SIRK formulas require function evaluations at times that are well in advance of $t = a + h$ for the higher stages. Thus, divergence of Newton's iteration (cf. (2.7)) can be expected without close initial guesses. This difficulty prompted Moore and Flaherty [20] to consider the reduced-order formula

$$\overline{\mathbf{W}}_{MF}(a + \theta h) = \sum_{k=1}^{s} \hat{\mathbf{W}}_k L_{k-1}(\theta/\lambda). \tag{4.1}$$

Unfortunately, neither $\overline{\mathbf{W}}_{BBC}(t)$ nor $\overline{\mathbf{W}}_{MF}(t)$ produced reliable solution estimates at advanced SIRK stages. Solutions $\overline{\mathbf{W}}(t)$ at $t = a + c_l h$, $l = 1, 2, \cdots, s$, appear to converge more rapidly than elsewhere on $t > a$. This suggests a modified Butcher (MB) strategy which generates initial guesses by (3.4) if $\theta \leq 1$ and by the solution at the closest SIRK stage of previous step if $\theta > 1$. Results of Moore and Flaherty [20] suggest that $\overline{\mathbf{W}}_{BBC}$ is more accurate than $\overline{\mathbf{W}}_{MF}$ when $\theta \leq 1$ and that the opposite is true when $\theta > 1$ and we call this the combination (CO) strategy. We use the initial data $\overline{\mathbf{W}}_0$ to provide Newton guesses for each stage as a benchmark (IC) strategy. A comparison of these strategies appears in Example 5.2.

4.2 Adaptive Strategies in Space. The solution of (2.7), the error estimates $\|\mathbf{E}^0(\cdot, a + c_l h)\|_{rms}$, $l \in \Gamma_s$, and the elemental spatial error estimates $\|\mathbf{E}^{x,k}(\cdot, a + c_l h)\|_{rms,i}$, $l \in \Psi_s$, $i = 1, 2, \cdots, N$, $k = -2, -1, 0, 1$ are computed for each time step. The largest "acceptable stage," $l_{\max} \in \Gamma_s$, for which $\|\mathbf{E}^0(\cdot, a + c_{l_{\max}} h)\|_{rms} \leq 1$ is determined and the time step is advanced accordingly; otherwise the step is rejected (cf. Figure 4.1). A new grid is always generated when a step is rejected or when a partial step is taken. A new grid may also be generated with a full step when significant refinement and/or coarsening is indicated. This must be done carefully since frequent regridding requires additional assemblies and

factorizations of functions and Jacobians. It also reduces the possibility of increasing the temporal order since such increases require two successive accepted steps with the same grid. However, only regridding when a step is rejected or a partial step is taken results in too many rejected steps and delays mesh coarsening (cf. Examples 5.1-5.3). Our compromise is to regrid on an accepted step when more than 50% of the elements should be coarsened or more than 5% should be refined.

The spatial error estimates $\|\mathrm{E}^{x,k}(\cdot,a + c_l h)\|_{rms,i}$, $l \in \Psi_s$, $i = 1, 2, \cdots, N$, $k = -2, -1, 0, 1$, are used to generate elemental refinement indicators $I_i^{x,k}$, $i = 1, 2, \cdots, N$, $k = -2, -1, 0, 1$, as described below. Once new orders $\hat{p}_i$ have been selected for each element, the mesh is modified so that $I_i^{x,\hat{p}_i - p_i} \approx 1/\sqrt{N}$, $i = 1, 2, \cdots, N$, and is, thus, equidistributed over the mesh. Specifically, each element is refined by 2^J where J is the smallest integer larger than $1/\hat{p}_i \log_2(\sqrt{N} I_i^{x,\hat{p}_i - p_i})$ for refinement and $J = -1$ for coarsening. The mesh is represented as a binary tree with finer elements created by refinement regarded as offspring of coarser ones. Coarsening of two adjacent elements at the same refinement level occurs only when they have the same parent and only when the local spatial indicator associated with each element i is less than $1/(5\times 2^{\hat{p}_i - 1}\sqrt{N})$.

The order selection strategy on element i is based on the size of $I_i^{x,0}$. If $I_i^{x,0} > 1/\sqrt{N}$, the order is changed if the sequence $I_i^{x,k}$, $k = -2, -1, 0, 1$ is increasing or decreasing. If $I_i^{x,0} < 1/(5\times\sqrt{N}\, 2^{p_i})$ and if $I_i^{x,-1} < 1/(5\times\sqrt{N}\, 2^{p_i})$ the order is too high and may be reduced by one, i.e, $\hat{p}_i = p_i - 1$. Finally, if the error on element i is "satisfactory" but either $I_i^{x,1} < 1/(10\times\sqrt{N}\, 2^{p_i})$ or $I_i^{x,-1} < 0.5/\sqrt{N}$ the order $\hat{p}_i$ is, respectively, increased or decreased by one. In all other cases, the order is unchanged. An increase in order should result in a coarser mesh which should reduce the dimension of the discrete system.

To ensure a "smooth" mesh gradation a 1-neighbor rule [4] is invoked with respect to step size and order; thus neighboring elements must differ in size by at most a factor of two and in order by at most one. The order smoothing was essential in solving Example 5.4.

The above spatial refinement strategy with $I_i^{x,k} = \|\mathbf{E}^{x,k}(\cdot, a + c_l h)\|_{rms,i}$, $k = -2, -1, 0, 1$, is referred to as the *base* strategy and is identified by the letter B. Several variations of Strategy B follow and these are compared in §5.

NG *No Grid-Prediction Strategy.* The grid is refined only when the prescribed error tolerance is exceeded.

FP *Full Prediction Strategy.* The idea of predicting where spatial refinement will be needed in subsequent time steps was introduced by Bietermann and Babuska [5] who utilized pattern recognition techniques and the extrapolation of data at previous times to predict future meshes. With SIRKs, solution information is available in advance of the accepted time step. In the full prediction strategy, we utilize spatial errors of other SIRK stages to select a grid for a subsequent time step. In particular, we set $I_i^{x,k} = \max_{l=l^*-1,l^*} \|\mathbf{E}^{x,k}(\cdot, a + c_l h)\|_{rms,i}$ if a step is rejected or a partial step is taken and $I_i^{x,k} = \max_{l=l^*,l^*+1} \|\mathbf{E}^{x,k}(\cdot, a + c_l h)\|_{rms,i}$ if a full step is taken, $k = -2, -1, 0, 1$.

NP *No Partial-Step Strategy.* Butcher [10] indicated that partial-step capabilities would be dropped from future versions of the SIRK code STRIDE because of its limited benefits and we seek to determine whether or not this applies in a MOL setting. Hence, Strategy NP uses Strategy FP but partial steps are not allowed.

SX *Szabo's Extrapolation Strategy.* Szabo [26] uses extrapolation of the spatial errors of solutions of local degrees p_i, $p_i - 1$, and $p_i - 2$ to construct an estimate of the error for an approximation of degree $p_i + 1$. This is straightforward if

$p_i > 2$. When $p_i = 2$, local solutions having degrees 2 and 1 are linearly extrapolated. When $p_i = 1$, we could either (i) obtain a "higher-order" solution by adding the spatial error estimate (cf. §3.2) to the linear solution on element i or (ii) construct a "lower-order" piecewise constant ($p_i = 0$) solution using the value of the piecewise-linear-solution at the center of subinterval i. Linear extrapolation is used in both cases. Results of both strategies were very similar and computations in §5 were obtained using the latter technique. We use SX with full prediction since this was significantly more efficient than strategies with no prediction.

These *hp*-refinement strategies are compared with several *h*-refinement strategies and a *p*-refinement strategy. The *h*-refinement strategies use the Strategy B with p fixed at 2, 3, 4, and 12. We refer to these strategies by their value of p. The *p*-refinement strategy uses a fixed uniform grid with p varying according to Strategy B and the proviso that p is increased by one when mesh refinement is needed on an element. Coarsening leads to a decrease of p by one.

A slight modification of Strategy B is used to select an initial grid for all *hp*-strategies. Beginning with an initial uniform grid of 20 elements and uniform order $p = 3$, up to ten iterations of the *p*-refinement algorithm just discussed are executed using Szabo's [26] *p*-refinement criterion. Elements that become linear during this process remain so; thus, there is no need for extrapolation. The iteration is continued until either the appropriate tolerance is satisfied on each element or the maximum number of iterations is reached. *H*-refinement is performed on the last iteration to get the initial grid.

Initial conditions between meshes of different dimension are obtained by first interpolating nodal values to the new mesh to obtain the piecewise linear approximation and then using a simplified energy projection to obtain the higher-order

coefficients. This procedure which only requires local computations, and is motivated by the following lemma.

Lemma 4.1. Let $q(x) \in H^{p+1}(\Omega)$ and $Q(x) \in S^{\Delta_\Omega}$ with $p_i = p$, $i = 1, 2, \cdots, N$, be such that

$$Q(x_i) = q(x_i), \tag{4.3a}$$

$$(q' - Q', V')_i = 0, \quad \text{for all } V \in S_0^{p,(x_i - x_{i-1})}, \tag{4.3b}$$

where

$$(W', V')_i = \int_{x_{i-1}}^{x_i} W'(x)V'(x)dx, \quad i = 1, 2, \cdots, N. \tag{4.3c}$$

If $k_i = x_i - x_{i-1}$ and $k_{\max} = \max\limits_{1 \le i \le N} x_i - x_{i-1}$ then

$$\|q(\cdot) - Q(\cdot)\|_1 \le Ck_{\max}^p \tag{4.3d}$$

where C is independent of the grid.

Proof. Let $W(x) \in S_E^{p,(x_i - x_{i-1})}$, i.e., $W(x_{i-1}) = q(x_{i-1})$ and $W(x_i) = q(x_i)$. Setting $V = W - Q \in S_0^{p,(x_i - x_{i-1})}$ and using (4.3b)

$$\|q' - W'\|_{0,i}^2 = \|q' - Q'\|_{0,i}^2 + \|V'\|_{0,i}^2. \tag{4.4}$$

Local Sobolev-space norms $\|\cdot\|_{p,i}$ are defined as their global counterparts [23] but are restricted to a subinterval (x_{i-1}, x_i). Neglecting the last term in (4.4) gives,

$$\|q' - Q'\|_{0,i}^2 \le \|q' - W'\|_{0,i}^2, \quad \text{for all } W \in S_E^{p,(x_i - x_{i-1})}. \tag{4.5}$$

Choosing $W(x) \in S_E^{p,(x_i - x_{i-1})}$ to be be an interpolant and using standard estimates [23] yields

$$\|q' - Q'\|_{0,i}^2 \le Ck_i^{2p}\|q\|_{p,i}^2 \tag{4.6}$$

where C is independent of k_i. Conditions (4.3) and use of the Schwarz inequality imply

$$\|q - Q\|_{1,i}^2 \leq Ck_i^{2p}\|q\|_{p,i}^2, \quad i = 1, 2, \cdots, N. \tag{4.7}$$

The result (4.3d) follows from a summation over i. □

A strategy similar to that used with BDF codes (cf., e.g., Shampine and Gordon [24]) is used to eliminate the need for a user-prescribed initial time step and order. The method begins with an order one SIRK, and increases the order by one and doubles the time step on successive steps until the tolerance is violated. Unlike Shampine and Gordon [24] instead of ending this initial integration phase if the temporal error is too large on the first time step, we make a second attempt with a time step selected to reduce the temporal error to 1/20 of the tolerance. This greatly improved the performance of the initial phase integration by allowing us to use higher-order methods in time more quickly than with Shampine and Gordon's [24] algorithm. To compare the two we also consider an additional Strategy ES.

ES *No Extra Startup Strategy*. Strategy FP is used with Shampine and Gordon's [24] initial integration strategy.

H-refinement is not allowed during this initial phase; thus, this phase could end prematurely if the initial mesh is inadequate.

5. Computational Results. Results of four examples demonstrate the performance of the adaptive *h*- and *hp*-refinement procedures. The first three examples are used to compare the various spatial refinement strategies; temporal enrichment remains invariant except for the acceptance or rejection of partial steps and the initial integration phase. Experimentation is restricted to the *hp*-refinement strategy in space (except where noted) since the properties of variable order-variable step SIRKs have been investigated elsewhere [8]. The latter two examples indicate that our general-purpose software can be used to solve realistic problems with no user intervention. All computations were performed in double precision on SUN 4/380 and SPARCstation II workstations. All timings were performed on SPARCstation II workstations.

Computational effort was measured by either (i) the total number of space-time unknowns including those for the error estimates or (ii) the CPU time to integrate to time T. For Strategy SX, the third solution (3.10) with $k = 1$ was not needed and this is reflected in the number of unknowns and the CPU time.

Example 5.1. Consider the linear heat conduction equation

$$u_t + f(x,t) = u_{xx}, \quad 0 < x < 1, \quad t > 0, \tag{5.1a}$$

with $f(x,t)$, the initial data, and the Dirichlet boundary conditions chosen so that the exact solution is

$$u(x,t) = 2.4\tanh 75(x + 1.4t - 1.4) - 2\tanh 100(x - t - 1/4). \tag{5.1b}$$

Thus, the solution represents two steep wave fronts moving in opposite directions that interact and pass through each other.

We solved this problem for $0 < t \le 0.7$ with $atol = 0.05/5^k$, $k = 0, 1, \cdots, 8$, and $rtol = 0$ using the various h- and hp-refinement strategies of §4. The global errors in the H^1 norm at $t = 0.7$ are presented as functions of the number of unknowns in Figure 5.1.

It is clear that Strategy FP is superior to the h-refinement Strategies 2, 3, and 4 even for large tolerances. The h-refinement Strategy 12 offers slightly better performance as a function of the number of unknowns but it frequently failed to reduce the error sufficiently when the tolerance was reduced. Since h-refinement only changes the number of elements by an integral amount, an order-12 method can drastically reduce the local error; thus, satisfying accuracy requirements for several tolerances. Strategy p was not able to solve (5.1) when $atol = 0.05/5^7$ and $0.05/5^8$.

The adaptive hp-refinement strategies, shown at the right and bottom of Figure 5.1, all produce comparable results for the larger tolerances and errors. Lower-order SIRKs are used with larger tolerances and any partial steps that are taken are only a

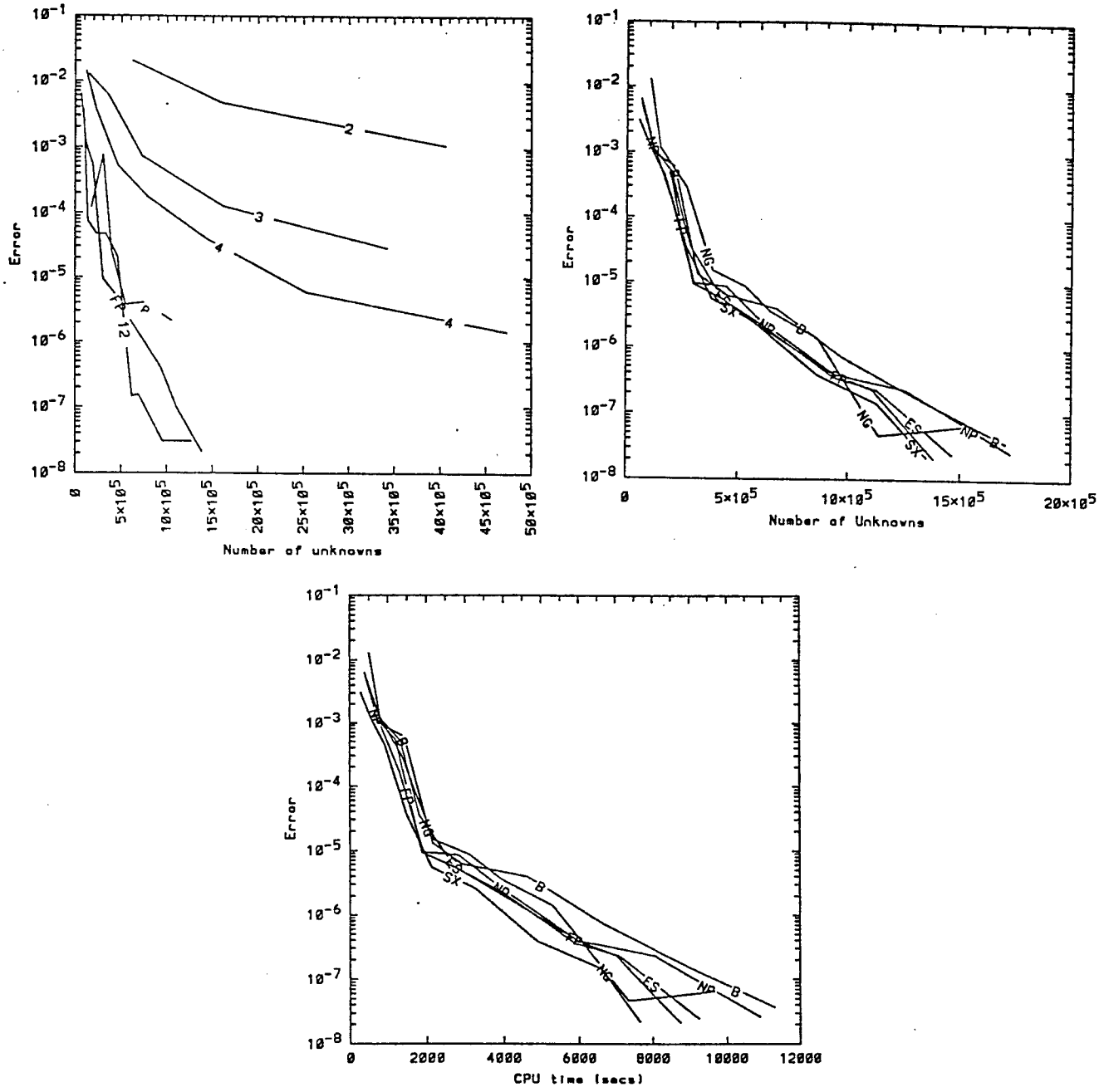

Figure 5.1. Global errors in the H^1 norm at $t = 0.7$ for Example 5.1 as a function of the number of unknowns for the Strategies FP, 2, 3, 4, 12, p, (upper left), and B, FP, SX, NP, NG, and ES (upper right). Global errors in the H^1 norm at $t = 0.7$ for Example 5.1 as a function of the CPU time for the Strategies B, FP, SX, NP, NG, and ES (bottom).

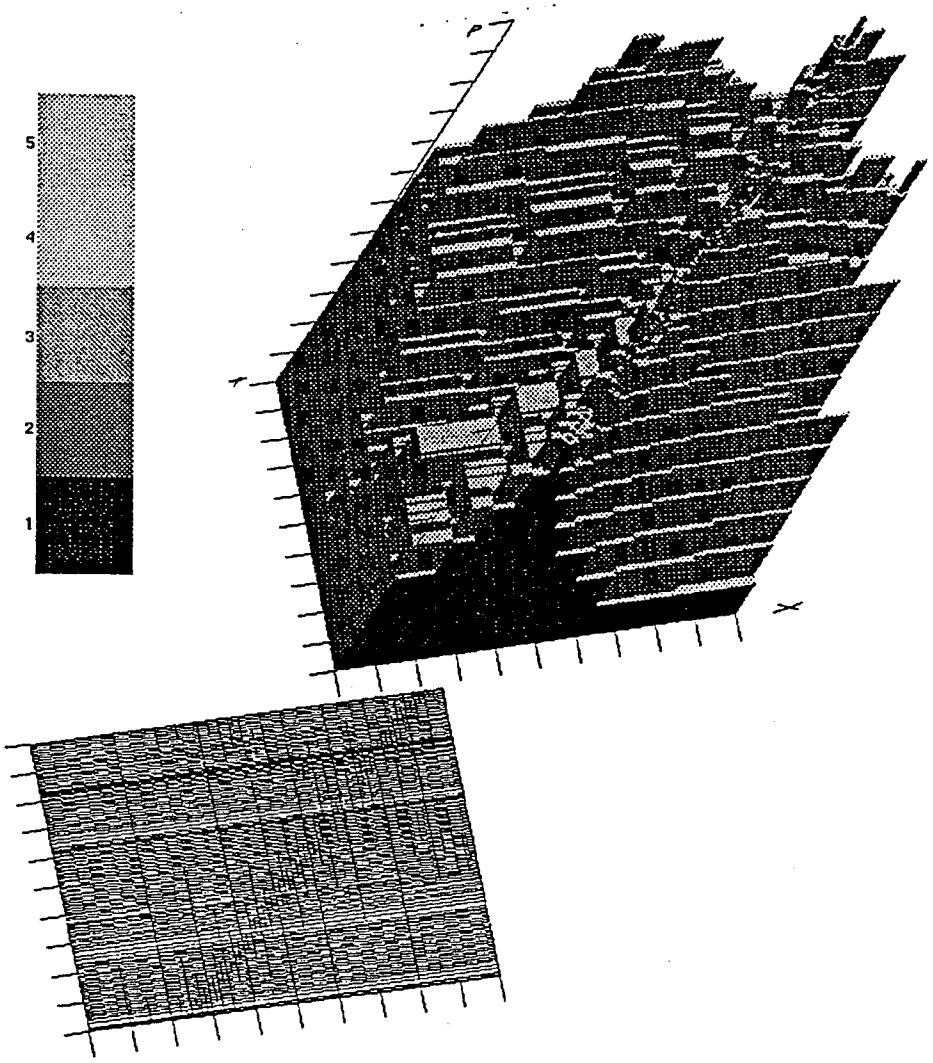

Figure 5.2. Grid and order used in solving Example 5.1 with Strategy FP with *atol* = 0.01. Temporal order is indicated by greyscale, and spatial order by height.

No. of stages *atol*	1	2	3	4	5	6	7	8
$0.01/5^1$	2,0	1,0	1,0	1,0	136,1	0	0	0
$0.01/5^2$	2,0	1,0	1,0	1,0	1,0	168,1	0	0
$0.01/5^3$	2,0	1,0	1,0	1,0	1,0	205,0	25,2	0
$0.01/5^4$	2,0	1,0	1,0	1,0	1,0	263,0	43,3	0
$0.01/5^5$	2,0	1,0	1,0	1,0	1,0	251,0	33,0	69,1
$0.01/5^6$	2,0	1,0	1,0	1,0	1,0	329,0	158,20	7,3
$0.01/5^7$	2,0	1,0	1,0	1,0	1,0	123,0	188,16	168,12
$0.01/5^8$	2,0	1,0	1,0	1,0	1,0	10,0	114,1	361,21

Table 5.1. The number of time steps and the number of partial time steps taken as a function of the number of stages and tolerance when Strategy FP is applied to Example 5.1.

atol Strategy	0.01	$0.01/5^1$	$0.01/5^2$	$0.01/5^3$	$0.01/5^4$	$0.01/5^5$	$0.01/5^6$	$0.01/5^7$	$0.01/5^8$
FP	1.4%	0.7%	0.6%	0.4%	0.6%	0.3%	0.4%	0.2%	0.6%
NG	4.0%	9.4%	6.2%	5.3%	3.0%	3.6%	4.9%	3.3%	2.1%

Table 5.2. Percentage of rejected steps when Strategies FP and NG are applied to Example 5.1.

small fraction of a potential full step. However, when the higher-order SIRKs are used with the smaller tolerances, there is a clear advantage of the partial-step strategies (e.g., FP and SX) relative to Strategy NP. Partial steps with the higher-order SIRKs may be as much as 40% of a potential full step. Table 5.1 indicates the number of time steps and the number of partial time steps that were taken at each SIRK order and each tolerance for Strategy FP. These results verify that the higher-order SIRKs are taking a sizable number of partial time steps.

At the smaller tolerances, Strategies FP and SX are clearly superior to B; thus, the ability to predict a future mesh is a definite advantage. Strategy ES is slightly less

efficient than FP at the smallest tolerances, but is otherwise comparable. Strategy NG has an undesirable erratic behavior as the tolerance is varied. Finally, the two complexity measures are comparable with Strategy SX being the most efficient relative to CPU time.

The percentage of rejected steps is shown as a function of tolerance for Strategies FP and NG in Table 5.2. Once again, the ability to predict future grids is valuable and has reduced the number of rejected steps.

The grid used to compute the solution using Strategy FP with $atol = 0.01$ is shown in Figure 5.2. The greyscale indicates the temporal order used and the height (p axis) indicates the spatial order. The grid and method order both track the steep fronts. After interaction, the fine grids separate following the individual waves. In this example the temporal order quickly climbs to five (during the initial phase) and remains there throughout the integration.

Example 5.2. Consider Burgers' equation

$$u_t + uu_x = \varepsilon u_{xx}, \quad 0 < x < 1, \quad t > 0, \tag{5.2a}$$

where ε and the initial and Dirichlet boundary conditions are chosen so the exact solution is

$$u(x,t) = 1-2\tanh 81(x - t + 1.3). \tag{5.2b}$$

This solution is, once again, a steep wave traveling in the positive x direction as time increases.

We solved this problem for $0 < t \leq 1.0$ with $atol = 5\times 10^{-k}$, $k = 0, 1, \cdots, 7$, and $rtol = 0$ using Strategy B and the time extrapolation strategies described in §4.1. The error in the H^1 norm is presented as a function of the number of unknowns in Figure

5.3. The three Strategies BBC, MF and CO are comparable for all but the smallest tolerance where BBC performs slightly better. Strategies IC and MB performed significantly worse than the other three. The optimal Newton initial guess strategy is dependent on both the problem and on the adaptive method used to solve it.

We also solved (5.2) for the same time interval and tolerances with the *hp*-refinement strategies of §4 and the "best" temporal extrapolation strategy. In the case of Strategies B, FP, SX, and NG, the best Newton guess strategy is BBC while NP works best with MF. The results, given in Figure 5.4, indicate that Strategies FP and SX are again clearly superior to NP and B. Strategy NG uses fewer unknowns for small tolerances but, the difference between it and Strategy FP as measured in CPU time is not significant. As in Example 5.1, Strategy NP is comparable to FP and SX for the large tolerances but becomes less efficient for small tolerances. Thus, accepting partial steps seems to be beneficial when solving partial differential equations to high accuracy. Strategies ES and FP produce identical results for this problem. In Table 5.3, we again verify that Strategy NG has rejected a larger percentage of steps than Strategy FP.

Example 5.3. Consider the Brusselator problem with diffusion [15]

$$u_t - 1 - u^2 v + 4.4u = \varepsilon u_{xx}, \tag{5.3a}$$

$$v_t - 3.4u + u^2 v = \varepsilon v_{xx}, \quad 0 < x < 1, \quad t > 0, \tag{5.3b}$$

$$u(x,0) = 0.5, \quad v(x,0) = 1 + 5x - \tanh(20x)/4 - \tanh(20(x-1))/4, \quad 0 < x < 1, \tag{5.3c}$$

$$u_x(0,t) = u_x(1,t) = v_x(0,t) = v_x(1,t) = 0, \quad t > 0. \tag{5.3d}$$

The boundary data prescribed for $v(x,0)$ is consistent with (5.3d).

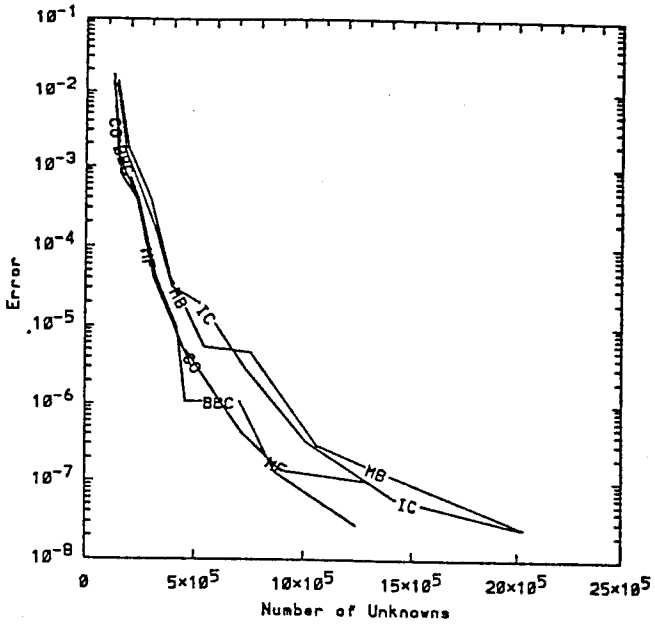

Figure 5.3. Global errors in the H^1 norm at $t = 1.0$ as a function of the number of unknowns when the Newton initial guess Strategies BBC, MF, CO, IC, and MB are applied to Example 5.2.

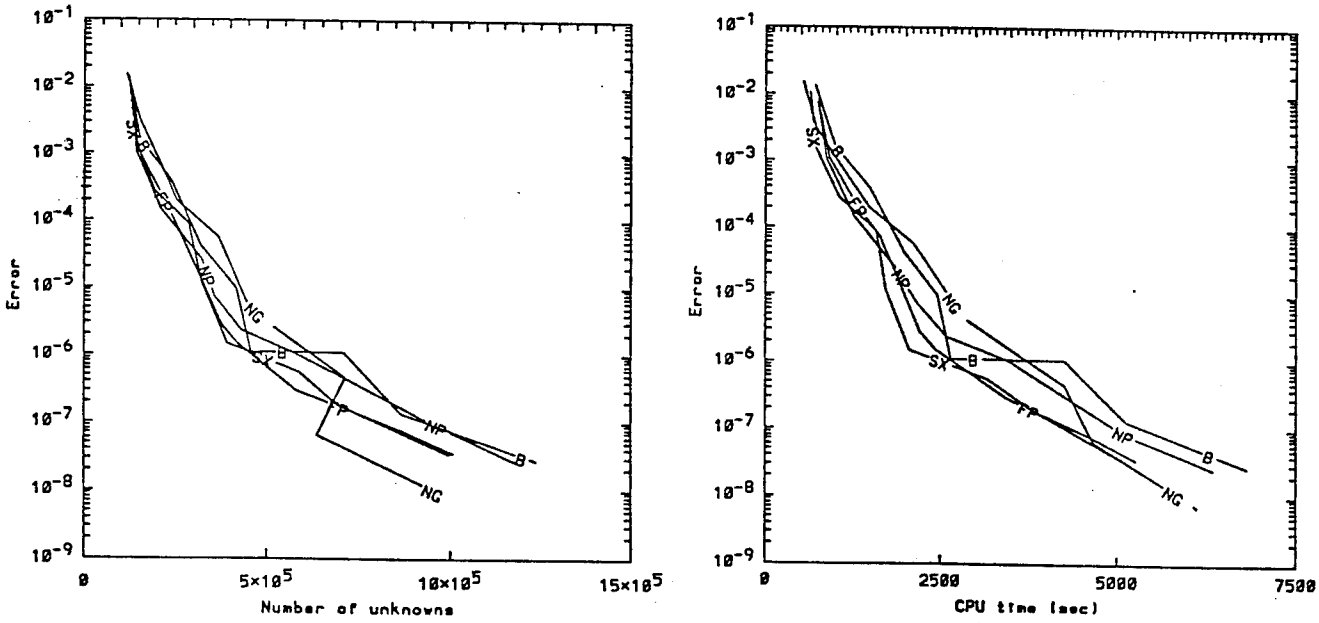

Figure 5.4. Global errors in the H^1 norm at $t = 1.0$ as a function of the number of unknowns (left) and CPU time (right) when Strategies B, FP, SX, NP, and NG are applied to Example 5.2.

atol Strategy	0.01	$0.01/5^1$	$0.01/5^2$	$0.01/5^3$	$0.01/5^4$	$0.01/5^5$	$0.01/5^6$	$0.01/5^7$	$0.01/5^8$
FP	10.3%	7.8%	5.5%	2.5%	3.5%	0.7%	1.2%	2.4%	0.5%
NG	11.6%	10.6%	10.0%	6.0%	4.9%	4.3%	6.0%	5.1%	2.4%

Table 5.3. Percentage of rejected steps when Strategies FP and NG are applied to Example 5.2.

We solved this problem for $0 < t \leq 12.6$ with $\varepsilon = 0.002$ and $atol^i = rtol^i = 0.05/5^k$, $i = 1, 2$, $k = 0, 1, \cdots, 8$, using Strategies B, FP, NG, SX, and ES with Strategy BBC. As an "exact solution," we used the results obtained from Strategy FP with $atol^i = rtol^i = 0.05/5^{13}$, $i = 1, 2$. The difference between this exact solution and a Strategy FP solution with $atol^i = rtol^i = 0.05/5^{12}$, $i = 1, 2$, is 5.38×10^{-9} in H^1. The H^1 error is shown as a function of the number of unknowns in Figure 5.5. The solution components at $t = 12.6$ exhibit steep fronts as shown in Figure 5.6. Unlike the previous examples, Strategy B performed better than Strategy FP for the larger tolerances; however, it exhibits some erratic behavior as the tolerance is varied. Strategy SX also exhibits some erratic behavior but is clearly superior to Strategy FP for the smaller tolerances. Strategies FP and SX are superior to and less erratic than Strategies B, NG, and NP at the smaller tolerances. Apparently, using advanced grid information to determine h-refinement has a smoothing effect on the convergence rate of the method. Strategies FP and SX also benefit from our modified initial integration phase.

The grid and method order used to calculate the solution on $0 < t \leq 12.6$ of (5.3) using Strategy FP with BBC and $atol^i = rtol^i = 0.01$, $i = 1, 2$, is shown in Figure 5.7. As in Example 5.1, the finest grids and highest order elements are concentrated near

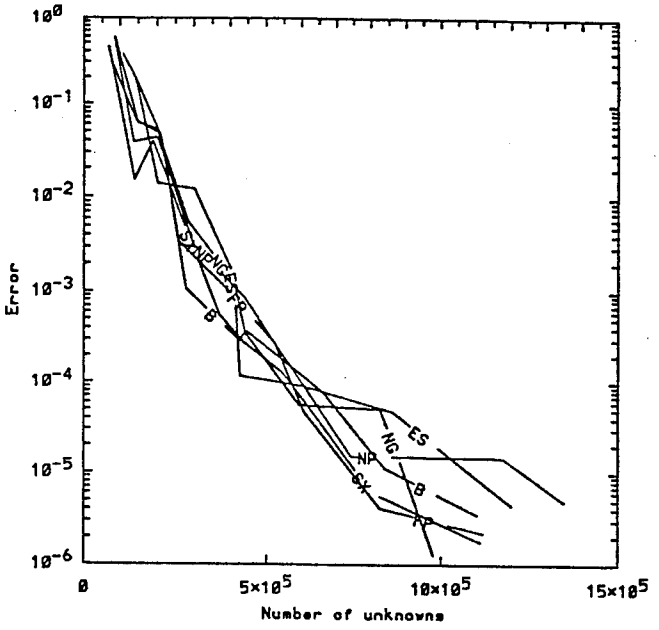

Figure 5.5. Global errors in the H^1 norm at $t = 12.6$ as a function of the number of space-time elements when Strategies B, FP, NG, SX, and ES with BBC are applied to Example 5.3.

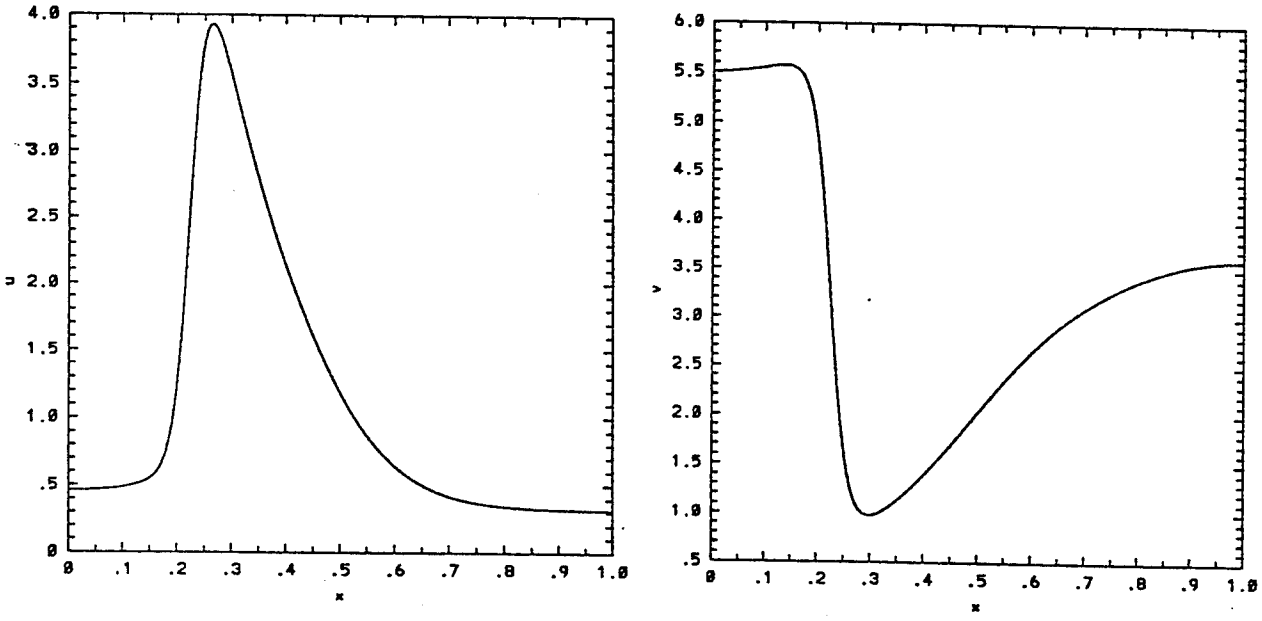

Figure 5.6. Solution components u (left) and v (right) at $t = 12.6$ obtained using Strategy FP with BBC and $atol^i = rtol^i = 0.05/5^5$, $i = 1, 2$.

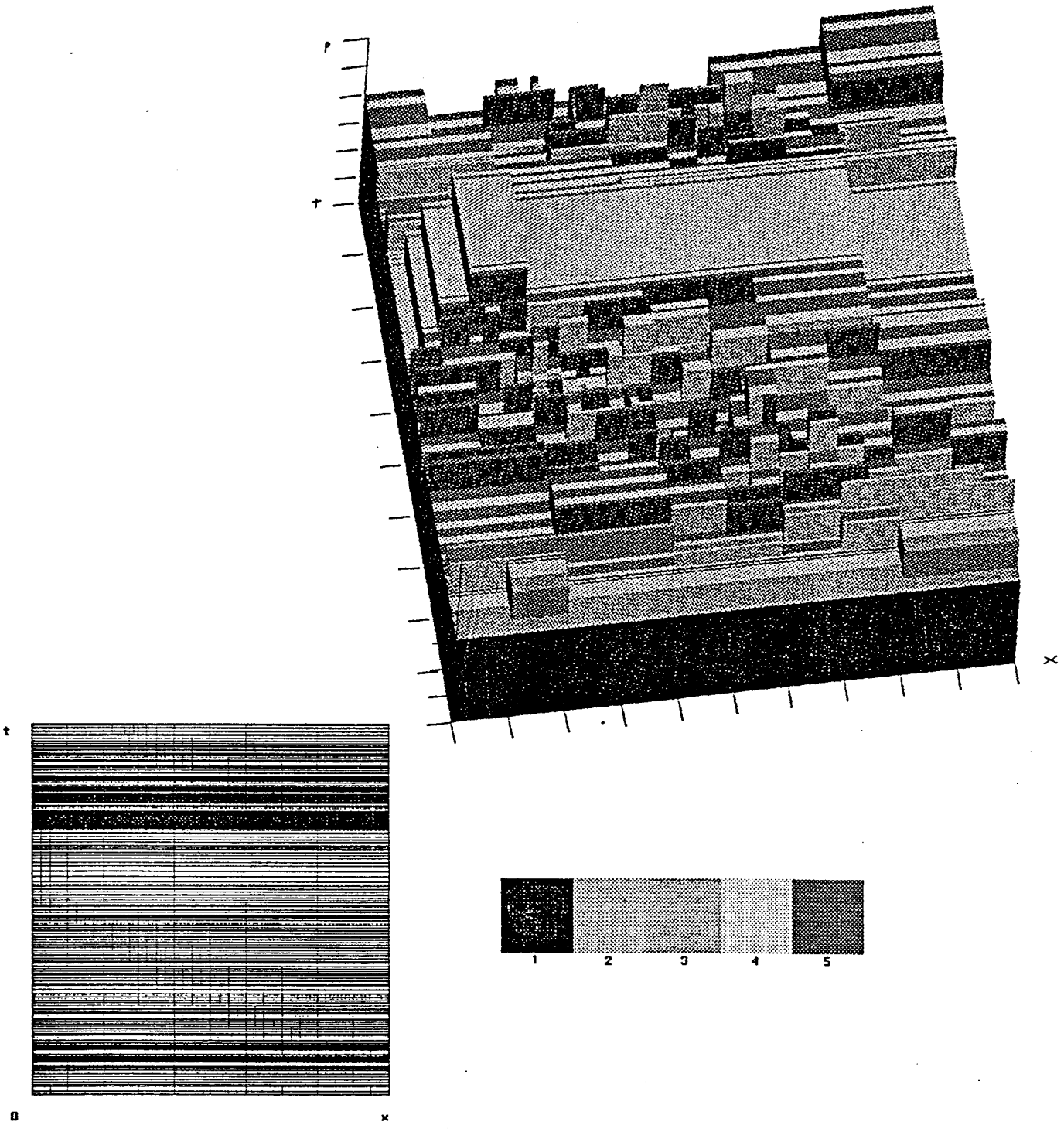

Figure 5.7. Grid and order used for Example 5.3 using Strategy FP with BBC and $atol^i = rtol^i = 0.01$, $i = 1, 2$. Temporal order is indicated by greyscale and spatial order by height.

the steep fronts.

Example 5.4. Consider the model of shear band formation introduced by Drew and Flaherty [12]

$$u_t - v = 0, \quad v_t = [G(T)u_x]_x + v_{xx}/Re, \tag{5.4a,b}$$

$$T_t - (v_x)^2/Re = T_{xx}/(PrRe), \quad 0 < x < 1, \quad t > 0, \tag{5.4c}$$

$$G(T) = 1/2[(1 + G_\infty) - (1 - G_\infty)\tanh((T - T_m)/\Delta T)], \tag{5.4d}$$

$$u(x,0) = v(x,0) = T(x,0) = 0, \quad 0 < x < 1, \tag{5.4e}$$

$$v(0,t) = 0, \; v(1,t) = V(t), \; T(0,t) = 0, \; T(1,t) = 0, \quad t > 0. \tag{5.4f}$$

This system describes the simple shearing of a slab of material having unit thickness. The variables u, v, and T denote the displacement, velocity, and temperature of the material point at the position x and time t. The shear modulus G depends on temperature according to (5.3d); thus, when $0 < \Delta T \ll 1$ the material undergoes a phase transition at the temperature T_m with the shear modulus abruptly changing from unity to G_∞. One edge ($x = 0$) of the slab is held fixed while the other ($x = 1$) is subjected to a shearing velocity $V(t)$. When $V(t)$ varies slowly, the velocity v is approximately a linear function of x; however, if $V(t)$ varies rapidly and the Prandtl number Pr and Reynolds number Re have appropriate values, the deformation will be localized in a narrow region called a shear band. Drew and Flaherty's [12] model (5.4) omits physical considerations which have been included in studies by Wright and Walter [28] and Walter [27]; however, (5.4) serves to illustrate that difficult nonlinear systems can be solved without a priori knowledge of solution behavior.

Consider a problem [12] with

$$V(t) = \begin{cases} V_0(t/r), & 0 < t < r \\ V_0, & r < d - r \\ V_0(d - t)/r, & d - r < t < d \\ 0, & d < t. \end{cases} \tag{5.4g}$$

The initial shearing velocity initiates a wave that propagates through the solid medium. The unloading at $t = d - r$ sends a second wave through the material. The passage of these waves generates heat which reduces the shear modulus. Sufficient heat can cause a phase transition to occur which can localize the deformation. In order to illustrate this, we performed a computation with $Re = 100$, $Pr = 50$, $G_\infty = 0.05$, $T_m = 0.03$, $\Delta T = 0.01$, $V_0 = 0.5$, $d = 1.5$, and $r = 0.05$ and solved (5.4) for $0 \le t \le 3.24$ with tolerances $atol^i = 0.01$ and $rtol^i = 0$, $i = 1, 2, 3$, using Strategy FP with BBC. Solutions are shown as functions of x for $t = 0.18$, 0.47, 0.78, 1.16, 1.46, 1.69, 1.95, 2.18, 2.65, and 3.08 in Figure 5.8. The space-time grid used for this calculation is shown in Figure 5.9. With this data, the temperature rises rapidly and a shear band forms in a layer adjacent to the loaded edge ($x = 1$). The grid is concentrated in the shear band region and follows its evolution into the domain. Initial orders increase quickly and then decrease where they are not needed for accuracy.

6. Discussion. We present and compare several adaptive *hp*-refinement strategies for solving parabolic systems. This investigation is much more extensive than previous studies [3, 19] which used larger tolerances and no grid prediction. It also unifies spatial and temporal enrichment to a much higher degree than was done previously. Spatial *hp*-refinement provides significant improvements in efficiency relative to *h*-refinement with either low- or moderate-order methods.

The differences in efficiency between the various *hp*-refinement strategies in space are not as great. Taking partial steps offers some advantages with small toler-

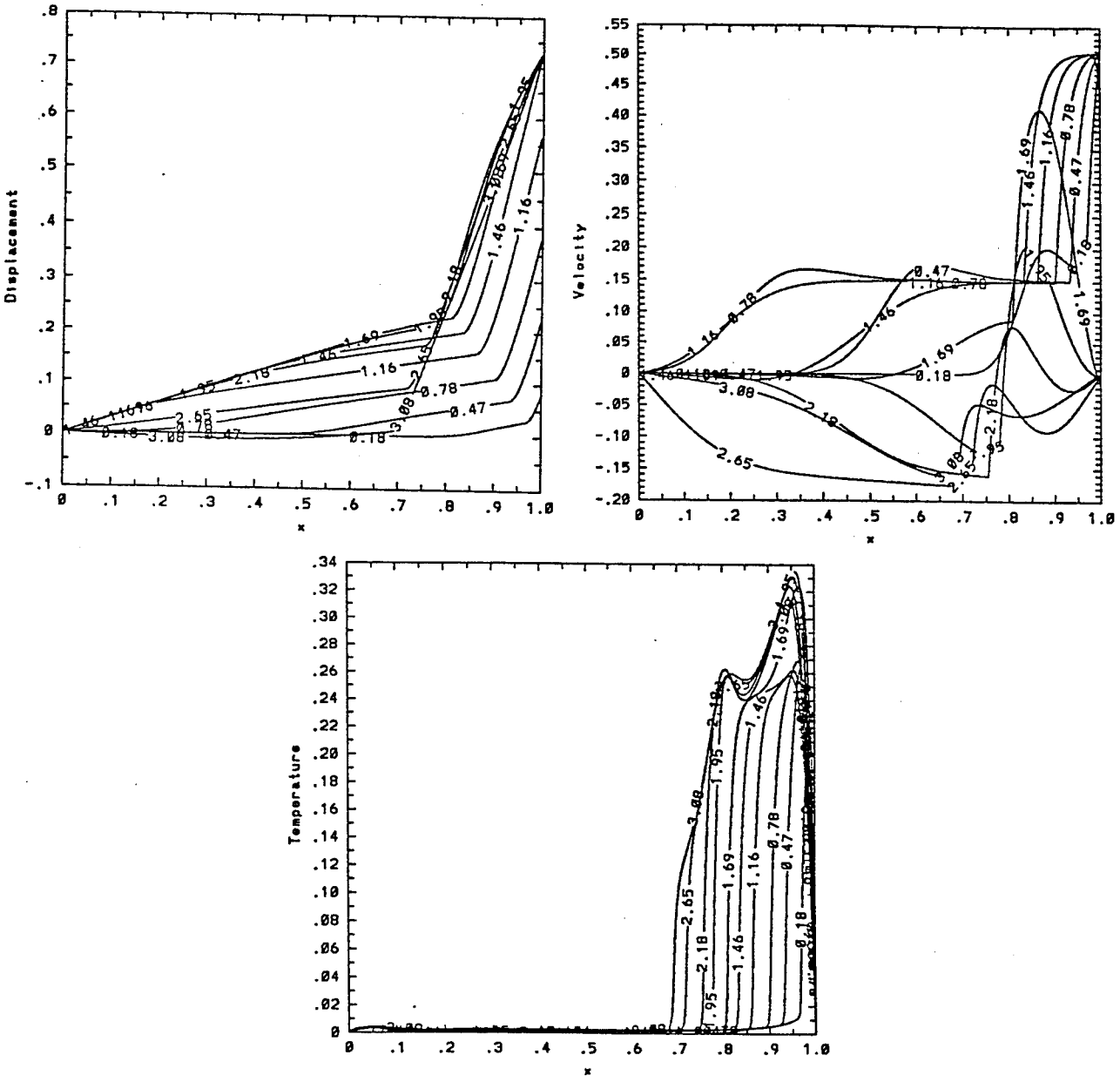

Figure 5.8. Displacement (upper left), velocity (upper right), and temperature (bottom) as functions of x for Example 5.4 at several times using FP with BBC and $atol^i = 0.01$, $rtol^i = 0$, $i = 1, 2, 3$.

ances and high-order methods. Grid prediction (Strategies B, FP, and SX) leads to a smoother relationship between the error and tolerance than no prediction (Strategy NG). Although Strategy SX outperformed Strategy FP in almost every case, indicating that extrapolation of low-order solutions can produce adequate indications of high-order error, it did exhibit some erratic behavior for large tolerances in Example 5.3. Further investigation is needed to clarify which is the better approach. In most cases

the number of unknowns and CPU time were comparable measures of work. However, there were exceptions in Example 5.1 with Strategy SX and in Example 5.2 with Strategy NP.

The three strategies for computing initial guesses for Newton's method, BBC, MF, and CO, were comparable with the best Newton guess strategy being dependent upon the adaptive strategy (cf. Example 5.2) and, clearly, the problem as well. The grids and orders selected according to Strategy FP successfully track important solution features. Examples 5.3 and 5.4 indicate that the adaptive *hp*-refinement strategies can robustly solve some difficult nonlinear systems with no user intervention.

Although no attempt was made to control the global temporal error, it appears that we have done so to a high degree. With stiff ordinary differential systems, such as those arising here, local errors do not accumulate [13, 17]; hence control of global errors is accomplished simply by controlling local errors.

Several issues remain. An alternative spatial error estimation strategy which involves solving local elliptic problems rather than local parabolic problems has been implemented in a MOL code which uses BDF formulas in time [3]. Reported gains in efficiency could be even greater with SIRKs since spatial error estimates are needed only at certain stages for the particular adaptive strategy used. Theoretical analysis of these estimates with SIRKs was done by Moore in [21] to show that they produce asymptotically correct results. A comparison of SIRK and BDF methods must be done. The BDF-based methods may outperform SIRKs at the larger tolerances but this may not be so for smaller tolerances. The strategies and software developed herein will be most helpful in developing multi-dimensional techniques.

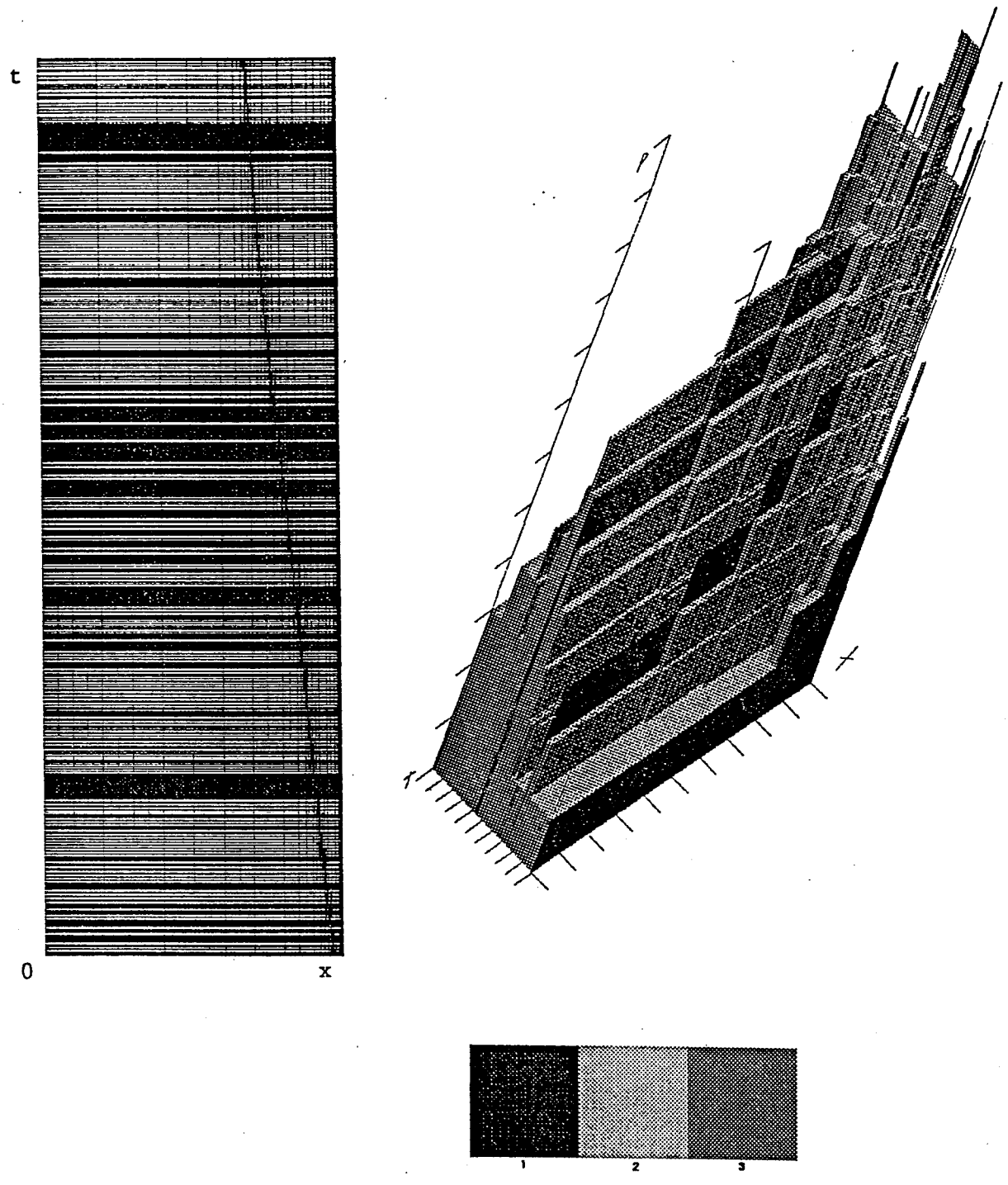

Figure 5.9. Grid on $0 \le t \le 3.24$ (left) and order on $0 \le t \le 0.38$ (right) used for Example 5.4 using Strategy FP with BBC and $atol^i = 0.01$, $rtol^i = 0$, $i = 1, 2, 3$. Temporal order is indicated by greyscale and spatial order by height.

REFERENCES

1. S. Adjerid and J.E. Flaherty, *A moving-mesh finite element method with local refinement for parabolic partial differential equations,* Comp. Meths. Appl. Mech. and Engrng. **55** (1986), pp. 3-26.

2. S. Adjerid, J.E. Flaherty, and Y. Wang, *A posteriori error estimation with finite element methods-of-lines for one-dimensional parabolic systems,* Tech. Report 91-1, Dept. Comp. Sci., RPI, Troy, NY 1991.

3. S. Adjerid, J.E. Flaherty, P.K. Moore, and Y. Wang, *High-order adaptive methods for parabolic systems,* Physica D **60** (1992) pp. 94-111.

4. R.E. Bank, *The efficient implementation of local mesh refinement algorithms,* in Adaptive Computational Methods for Partial Differential Equations, I. Babuska, J. Chandra, and J.E. Flaherty, Eds., SIAM, Philadelphia, (1983), pp. 74-81.

5. M. Bieterman and I. Babuska, *The finite element method for parabolic equations, II a posteriori error estimation and adaptive approach,* Numer. Math. **40** (1982), pp. 373-406.

6. K.E. Brenan, S.L. Campbell, and L.R. Petzold, *Numerical Solution of Initial-Value Problems in Differential-Algebraic Equations,* North Holland, New York, 1989.

7. K. Burrage, *A special family of Runge-Kutta methods for solving stiff differential equations,* BIT **18** (1978), pp. 22-41.

8. K. Burrage, J.C. Butcher, and F.H. Chipman, *An implementation of singly-implicit Runge-Kutta methods,* BIT **20** (1980), pp. 327-340.

9. J.C. Butcher, *A transformed implicit Runge-Kutta method,* J. A.C.M. **26** (1979), pp. 731-738.

10. J.C. Butcher, personal communication, 1992.

11. K. Dekker and J.G. Verwer, *Stability of Runge-Kutta Methods for Stiff Nonlinear Differential Equations,* Elsevier Science, Amsterdam, 1984.

12. D.A. Drew and J.E. Flaherty, *Adaptive finite element methods and the numerical solution of shear band problems,* in Phase Transformations and Material Instabilities in Solids, M.E. Gurtin, ed., Academic Press, Orlando, FL 1984, pp.37-60.

13. K. Eriksson and K. Johnson, *Adaptive finite element methods for parabolic problems I: a linear model problem,* SIAM J. Numer. Anal. 28 (1991), pp. 43-77.

14. W. Gui, and I. Babuska, *The h, p and h-p versions of the finite element method in 1 dimension,* Numer. Math. **49** (1986), pp. 659-683.

15. E. Hairer, S.P. Norsett, and G. Wanner, *Solving Ordinary Differential Equations I Nonstiff Problems,* Springer-Verlag, Berlin, 1987.

16. I.W. Johnson, M.J. Baines, and A.J. Wathen, *Moving finite element methods for evolutionary problems, II. applications,* J. Comp. Phys. **79** (1988), pp. 270-296.

17. J. Lawson, M. Berzins, and P.M. Dew, *Balancing space and time errors in the method of lines,* SIAM J. Sci. Stat. Comput. **12** (1991), pp. 573-594.

18. P.K. Moore and J.E. Flaherty, *A local refinement finite element method for one-dimensional parabolic systems,* SIAM J. Numer. Anal. **27** (1990), pp. 1422-1444.

19. P.K. Moore and J.E. Flaherty, *An hp-adaptive method in space and time for parabolic equations,* in Advances in Computer Methods for Partial Differential Equations VII, R. Vichnevetsky, D. Knight, and G. Richter, Eds., IMACS, Rutgers, (1992), pp. 532-538.

20. P.K. Moore and J.E. Flaherty, *High-order adaptive finite element-singly implicit Runge-Kutta methods for parabolic differential equations,* BIT. (1993), to appear.

21. P.K. Moore, *A posteriori error estimation with finite element semi- and fully-discrete methods for nonlinear parabolic equations in one space dimension,* SIAM J. Num. Anal. (1993), to appear.

22. S.P. Norsett, *Runge-Kutta methods with a multiple real eigenvalue only,* BIT **16** (1976), pp. 388-393.

23. J.T. Oden and J.N. Reddy, *An Introduction to the Mathematical Theory of Finite Elements,* John Wiley and Sons, New York, 1976.

24. L.F. Shampine and M.K. Gordon, *Computer Solution of Ordinary Differential Equations,* W.H. Freeman and Co., San Francisco, 1975.

25. B. Szabo and I. Babuska, *Introduction to Finite Element Analysis,* John Wiley and Sons, New York, 1989.

26. B. Szabo, *Mesh design for the p-version of the finite element method,* Comput. Meth. Appl. Mech. Eng. **55** (1986), pp. 181-197.

27. J.W. Walter, *Numerical experiments on adiabatic shear band formation in one dimension,* Tech. Report BRL-TR-3381, Ballistic Research Laboratory, Aberdeen Proving Ground, Maryland, 1992.

28. T.W. Wright and J.W. Walter, *On stress collapse in adiabatic shear bands,* J. Mech. Phys. Solids **35** (1987), pp. 701-720.

29. O.C. Zienkiewicz, J.Z. Zhu, and N.G. Gong, *Effective and practical h-p-version adaptive analysis procedures for the finite element method,* Int. J. Numer. Meth. Eng. **28** (1989), pp. 879-891.